

Article

Defect Modes Generated in a Stack of Spin-Coated Chiral Liquid Crystal Layers

Frederik Van Acker ¹, Bo-Han Lin ², Chun-Ta Wang ², Kristiaan Neyts ³ and Jeroen Beeckman ^{1,*}

¹ Department of Electronics and Information Systems (ELIS), Ghent University, Technologiepark 126, 9052 Ghent, Belgium; frederik.vanacker@ugent.be

² Department of Photonics, National Sun Yat-sen University, Kaohsiung 804201, Taiwan; dick11416@gmail.com (B.-H.L.); ctwang@mail.nsysu.edu.tw (C.-T.W.)

³ State Key Lab of Advanced Displays and Optoelectronics Technologies, Hong Kong University of Science and Technology, Hong Kong; eeneys@ust.hk

* Correspondence: jeroen.beeckman@ugent.be; Tel.: +32-9-264-3337

Abstract: Nematic chiral liquid crystals (CLCs) are characterized by a helical arrangement of nematic LC molecules. A layer of CLC typically exhibits an optical reflection band due to Bragg reflection in the helical structure. When several layers of CLC are spin-coated and polymerized on top of each other without a barrier layer in between, defect modes can form in their reflection spectrum. By comparing experimental results and simulations, we investigate the origin of the defect modes, thereby revealing details on the behavior of the materials at the interfaces during deposition. Simulations show that these defect modes can originate from the migration of chiral dopant leading to a layer with a smaller pitch or from a discontinuity in the director orientation at the interface between two layers.

Keywords: CLC; PCLC; polymerized chiral liquid crystal; defect modes; diffusion; blue shift



Citation: Van Acker, F.; Lin, B.-H.; Wang, C.-T.; Neyts, K.; Beeckman, J. Defect Modes Generated in a Stack of Spin-Coated Chiral Liquid Crystal Layers. *Crystals* **2024**, *14*, 231. <https://doi.org/10.3390/cryst14030231>

Academic Editor: Ingo Dierking

Received: 14 February 2024

Revised: 23 February 2024

Accepted: 24 February 2024

Published: 28 February 2024



Copyright: © 2024 by the authors. Licensee MDPI, Basel, Switzerland. This article is an open access article distributed under the terms and conditions of the Creative Commons Attribution (CC BY) license (<https://creativecommons.org/licenses/by/4.0/>).

1. Introduction

Nematic chiral liquid crystals (CLCs) are liquid crystalline materials with a helical symmetry [1]. The thickness corresponding to a full 2π rotation of the director is called the pitch P . The local optical axis in a liquid crystal (associated with the extra-ordinary refractive index) is parallel to the average orientation of the long axes of the molecules, which is denoted by the director \vec{L} . The director of the liquid crystal remains parallel to the plane that is perpendicular to the helical axis, and the structure has a period of $0.5P$. This periodicity makes the CLC a 1-D photonic crystal. Photonic crystals find their applications in various fields, such as lasers, sensors, imaging, waveguiding, etc., and can be 1-, 2-, or 3-dimensional [2,3]. Their characteristics are based on a forbidden region or band gap for photons, which is a consequence of their periodicity. An important advantage of photonic crystals over homogeneous bulk materials is the freedom of design. By selecting the periodicity and materials, the reflection and polarization characteristics can be tailored to fit their purpose, but their fabrication for visible or near-infrared wavelengths is not always straightforward as it involves sub-micron material structuring.

An advantage of CLCs over most other photonic crystals is their ability to self-assemble spontaneously. A chiral dopant is added to a liquid crystal that will force the molecules to orient into a helix. The pitch of the helix is directly related to the concentration of the chiral dopant c by the following relation: $P \times c \times \text{HTP} = 1$ [4]. In this equation, HTP is the helical twisting power, a value depending on the dopant and on the liquid crystal material.

Assuming that the CLC is uniform and the director is oriented in-plane, the optical properties are fully determined by its optical anisotropy or birefringence ($\Delta n = n_e - n_o$), the average refractive index ($n_{avg} = \frac{n_e + n_o}{2}$), the handedness, and the pitch. The refractive indices are mainly determined by the liquid crystal host material (provided that c is not

too high) and the handedness by the chiral dopant. This means that P (through the concentration c) is the main design parameter of the CLC. When using non-reactive mesogens, the CLC layer remains liquid and is typically contained between two glass plates. When using reactive mesogens, for example, with acrylate end groups, the CLC layer can be photopolymerized and turned into a solid polymer film called a PCLC.

A CLC has an optical band gap centered around the wavelength $n_{avg} \times P$ with a width of $\Delta n \times P$. In this band gap, circularly polarized light with the same handedness as the CLC helix is reflected with conservation of its handedness while the other circular polarization is transmitted.

The excellent optical characteristics and spontaneous self-assembly make CLCs promising for applications such as RGB filters for displays [5], lasers [6–9], and gratings [10]. PCLC films are often made by polymerization between two glass plates. If further processing is needed, the cell has to be opened [11], which is difficult to incorporate in an automated process flow. This step can be avoided by spin-coating the CLC layer but with the trade-off that thicker layers are difficult to make. The layer thickness is limited by the solubility of the CLC in the spin-coating solvent, and as a result, the viscosity of the solution. A single layer thickness of $3.8 \mu\text{m}$ has been demonstrated in the literature [12], but to ensure sufficient optical quality layer thicknesses are usually limited to much lower values. A minimal layer thickness and a sufficient number of pitches in the layer is important to ensure a sufficiently high reflection and a well-defined band gap. This is important in various applications, such as low threshold CLC lasers [13] and color filters. The influence of the number of pitches on the optical reflection spectrum is shown in Figure 1a for perpendicular incidence, and for the following parameters: $P = 376 \text{ nm}$, $n_e = 1.687$ and $n_o = 1.508$. Such a spectrum can be calculated using an analytical equation based on coupled mode theory [14]. In this work, instead, a numerical method based on the Berreman method is used for calculating the reflection spectra [15]. It is clear from Figure 1a that no defect modes appear when extra pitches are added and the layer exhibits uniform behavior in terms of refractive indices and twisting.

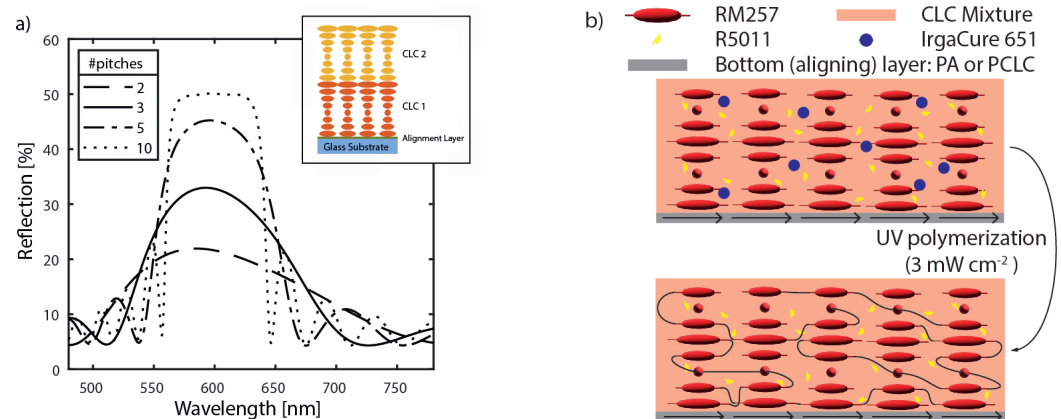


Figure 1. (a) CLC reflection spectra for different numbers of pitches. Inset: Structure of an ideal CLC structure based on two identical layers. (b) Schematic illustration of the deposition process for one polymerized CLC layer. The top figure illustrates the situation after spin-coating and before UV polymerization. The bottom figure illustrates the situation after polymerization.

A second complexity of spin-coating and photopolymerization is anchoring of the liquid crystal at the boundaries. In a layer sandwiched between glass plates, the liquid crystal is aligned at the top and bottom due to the presence of alignment layers, thereby guaranteeing planar alignment at the bottom and top due to the typical strong anchoring induced by the alignment layers. This forces the whole CLC to orient in-plane and enhances the uniformity of the layer. For spin-coated layers, it has been reported that the top LC-air

interface may induce a weak homeotropic alignment, which leads to a non-negligible out-of-plane tilting of the director [16].

The limitation in thickness can be solved by spin-coating several layers on top of each other. If these layers form a uniform layer without discontinuities, schematically shown in the inset of Figure 1a, an ideal band gap can be achieved with a spectrum resembling the ones in Figure 1a, but if the periodicity of such a periodic layer is broken, defect modes [17] form in the band gap. Because the helix has to be continuous, no barrier layers nor new alignment layers can be used in between the spin-coated CLC layers. The newly spin-coated layers' boundary conditions have to be enforced by the old layer and the new layer should not alter the previous one, otherwise defects may occur. The solvent in which the CLC is dissolved for spin-coating plays a crucial role as it may affect the underlying layer, and different physical effects may occur, such as dissolving the existing layer, diffusion of molecules from the existing layer into the solvent, swelling, etc.

Defect mode structures are not necessarily unwanted and have applications in defect mode lasers [18–20] and RGB reflectors [21–25]. Defect mode lasers can have a lower lasing threshold than CLC band edge lasers of the same CLC thickness. By using defect structures, RGB reflectors can be made from a single solution, which simplifies manufacturing. To make CLCs with a defect mode, a barrier layer between two spin-coated layers can be used or several PCLCs can be combined through bonding after polymerization [26].

In this work, we focus on CLC stacks with a defect that has been produced from a single polymerizable mixture. We aim to understand the origin of experimentally observed defect modes in order to avoid them or to design a CLC with defect modes made out of one CLC solution and without the need of additional layers in between. Therefore, we simulate the reflection spectra of CLC stacks with different deviations from the ideal structure and fit them to the experimental data. We start from a fit of the experimental reflection spectrum for a single layer CLC.

2. Materials and Methods

The chiral liquid crystal mixture is prepared by adding 1.8 or 2.8 wt% chiral dopant R5011 (HCCH, China, Nanjing) to RM257 ($n_e = 1.687$ and $n_o = 1.508$, from [11]; HCCH, Nanjing, China) in order to obtain a reflection band in the red, green, or blue region of the spectrum. An amount of photo-initiator IrgaCure 651 (HCCH, China, Nanjing) is added to the mixture with a 1:20 weight ratio. The obtained CLC mixture is subsequently mixed with toluene (Echo Chemical Co., Taiwan, Toufen City) and filtered with a syringe filter. Different CLC:toluene fractions by weight, going from 1:4 to 1:9, are used to obtain different CLC layer thicknesses after spin-coating.

The test samples are prepared by first spin-coating an SD-1 [27] (DIC. Corporation, Japan, Tokyo) photoalignment layer on top of a blank glass substrate and illuminating it with linearly polarized blue light to define a homogeneous alignment at the surface. On top of the alignment layer, the CLC:toluene mixture is spin-coated at 5900 rpm during 90 s. After evaporation of the toluene during a soft bake at 90 °C, and cooling to room temperature, the CLC layer is polymerized by UV illumination for 30 min with a total dose of 5.4 J/cm². This is illustrated in Figure 1b. After the CLC layer has been polymerized, additional CLC layers can be deposited by repeating the same procedure (spin-coating, cooling, and polymerization). Samples with one, two, and three CLC layers have been prepared.

Mixtures with different amounts of chiral dopant are used to obtain a reflection band in the blue, green, or red part of the spectrum. These CLC mixtures are dissolved in toluene with different concentrations and this is performed for each color. Of each color/dilution combination, five samples are prepared to verify the reproducibility of the fabrication procedure (see Supplementary Materials, Figure S3). We only fitted the red and the green CLC of the highest concentration (CLC:toluene, 1:4). The blue spectra were omitted because the spectra showed too much noise below 400 nm (see Supplementary Materials, Figure S1) to have a meaningful fit and thinner layers had similar but less pronounced features making it more difficult to fit. The different spectra from the same mixture corresponded well

with each other. This leads to the six reflection spectra shown in Figure 2. The spectrum is obtained using perpendicularly incident unpolarized light.

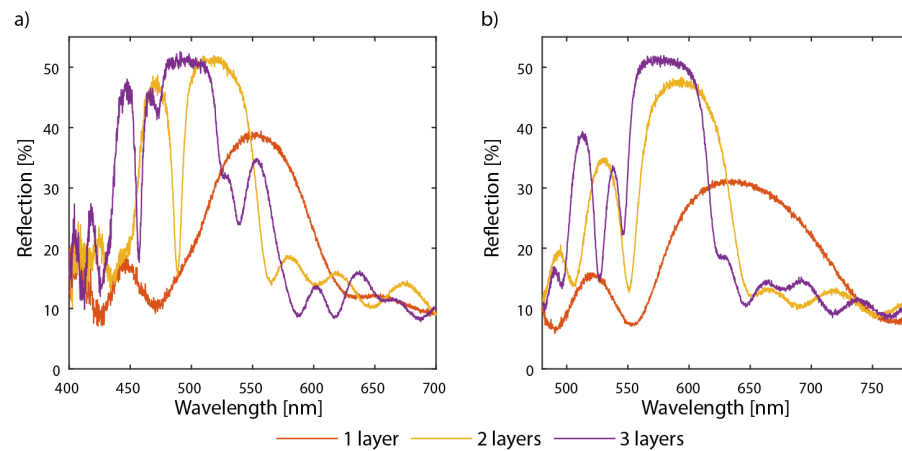


Figure 2. Measured reflection spectra for one, two, or three spin-coated CLC layers: (a) based on CLC with band gap in green, and (b) based on CLC with band gap in red.

The numerical simulations are based on the Berreman method as mentioned in the introduction. This is performed by approximating the CLCs by a number of uniaxial layers, each rotated over a fixed angle with respect to the previous one. The pitch is determined by the thickness of each of those layers.

3. Results

As expected, the maximum reflectivity increases with the number of layers in the CLC stack. Also, the sharpness of the edges increases. This can be explained by the increase in thickness of the stack. On the other hand, there are also a few deviations from the ideal case, shown in Figure 1a. In the reflection spectra for the CLC stacks with more than one layer, the band gap shifts to shorter wavelengths for an increasing number of layers. For the samples with two or three layers, the reflection spectrum is asymmetric, with one or two minima near the left side of the reflection band.

In order to find the origin of the variations in the experimental reflection spectra, we carry out numerical simulations and subsequently fit them to the experimental data.

3.1. Single Layer Devices

The first simulation result is based on a perfect CLC with the following values: $n_e = 1.687$, $n_o = 1.508$ and with 2, 3, 5 or 10 pitches. The pitch is assumed to be 376 nm and the director remains parallel to the substrate surface. The reflection spectrum shown in Figure 1a shows that the reflectivity increases with the number of pitches and reaches a value of close to 50% when there are 10 pitches. As the reflectivity increases, the edges of the band gap become steeper and better defined, leading to a smaller bandwidth. A third effect of the thickness on the reflection spectra is the decrease in spacing between the fringes next to the band gap as the CLC becomes thicker.

The measurements with only the first layer are used to estimate the thickness and the pitch of each individual layer. By focusing on the position of the band gap and the distance between the fringes, we obtain an estimate for the pitch and thickness of the red and green CLCs. Figure 3a,b show that there is a good match between the experimental and simulated spectra. A pitch of 403 nm and a thickness of 1.23 μm (or 3.1 pitches) are obtained for the red CLC. The thickness of the green CLC is assumed to be the same as the red CLC and the pitch is estimated to be 347 nm, which leads to 3.5 pitches. These parameters are then used as the basis for the 2-layer stacks.

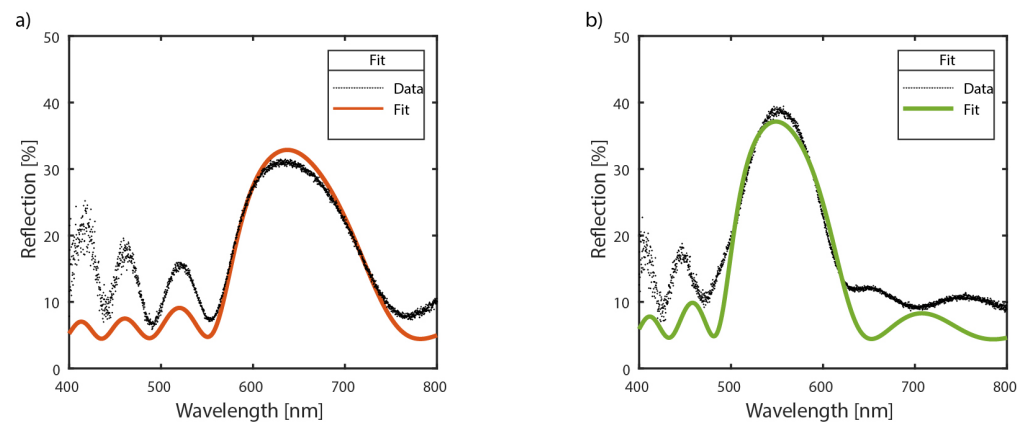


Figure 3. Reflection spectra for the case of only one spin-coated layer for the red CLC (a) and the green CLC (b). The experimental data are in black and the simulated spectra in red or green. The simulated spectra are based on a fitting procedure.

3.2. Two-Layer Devices

After spin-coating the second layer, two deviations from the ideal CLC are observed in the experimental data: a blue shift of the spectrum and the formation of a defect mode.

3.2.1. Origin of the Blue Shift

Since the position of the reflection band is governed by the average refractive index multiplied with the pitch, a blue shift should be explained by a change in one of those parameters.

First, we look into the effect of a mismatch in the position of the band gaps in a two-layer stack. This mismatch is simulated by changing the pitch (Figure 4a) or the refractive indices (Figure 4b) of layer 1 and keeping both CLCs uniform without discontinuities in director orientation at the interface. Layer 2 in both simulations is simulated with 10 pitches and the same parameters as the CLCs in Figure 1a. Layer 1 is identical to layer 2 except for the pitch in Figure 4a, which is 336 nm, or for the refractive indices in Figure 4b, which are $n_e = 1.481$ and $n_o = 1.356$. We chose to increase the number of pitches in the simulation to 10 to exclude the effect of a higher reflection where the band gaps overlap. This would interfere with illustrating the envelope of the two reflection bands.

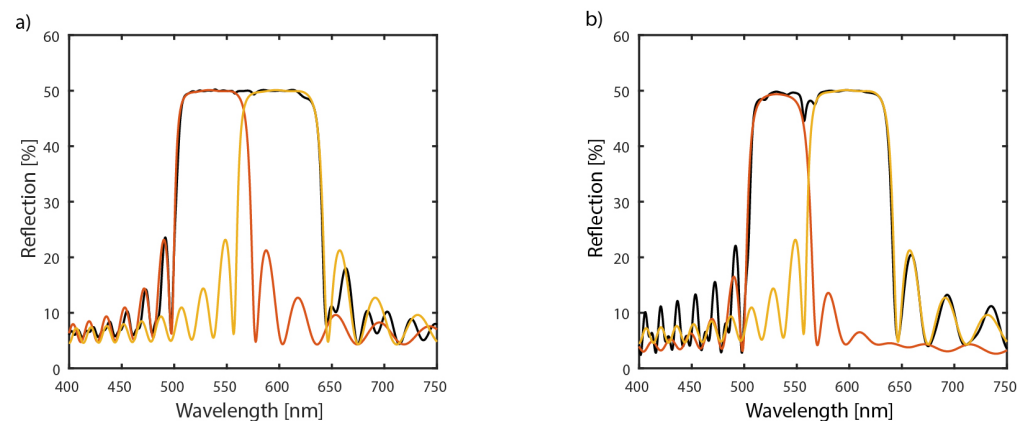


Figure 4. The simulated effects of changes in pitch or refractive index of a layer. The red spectrum corresponds with the spectrum of the bottom layer, the yellow spectrum with the top layer and the black spectrum with the 2 layers combined. (a) The reflection spectrum of 2 layers, where the pitch of the bottom layer shifted 40 nm to the blue. (b) The reflection spectrum of 2 layers, where the refractive indices n_e and n_o of the bottom layer decreased to 1.481 and 1.356.

The resulting spectra for the two-layer stack are shown in Figure 4, together with the spectra of the two individual layers. The reflection band is broadened considerably but no defects can be observed in the spectrum. This demonstrates that a mismatch in the band gap between the two layers alone cannot explain the appearance of a defect mode. Other structural changes in the layers need to be present.

In our fitted models, we assumed that no material can leave the sample once the spin-coat step is finished. For that reason, the thickness of the second layer is increased to compensate for the loss in thickness in the first one after the pitch change.

The change in central wavelength could be explained by the fact that a fraction of the material from layer 1 is washed out during the second spin-coating step because it might not have been fully polymerized. If the density remains the same, the CLC shrinks and, in this case, the pitch should decrease. If the thickness remains the same and the remaining monomers are washed away by the solvent, the density decreases and the layer becomes more porous. This would result in a decreased optical thickness and, as a result, a decreased refractive index. Both mechanisms could also occur at the same time. The blue shift of layer 2 could originate from the migration of a fraction of the chiral dopant from the bottom layer to the top layer after coming in contact with the solvent during the second spin-coating step.

3.2.2. Twist Defect

A possible cause of the defect mode is a twist defect [28], which forms when there is a discontinuity in the twist angle inside a CLC. This is schematically represented in Figure 5a. The resulting transmission spectra are simulated in Figure 5b. The parameters of the two CLCs are the same as those in Figure 1a, with three pitches for each CLC. The spectrum shows a defect mode, the position of which is determined by the discontinuity in the twist angle.

The position of the defect mode has an important effect on the amplitude of the reflection band near the defect mode. This effect becomes less important when the number of pitches increases, because the reflection coefficient of the reflection bands will, in that case, be close to 0.5.

The fitting procedure consisted of fitting the minima at the short band, the defect mode, and the long band of the experiments to the simulations and subsequently applying a least square method to the data in the band gap to improve the fit.

In Figure 5c,d, the best fits according to the twist defect model are shown, together with the measured spectra. The fitting parameters are given in Table 1, with $\Delta\phi$ the discontinuity in twist. This angle was varied for the red CLC and the green CLC. The simulations fitted the results in an interval of about 5° and the angle was then fixed in this interval. P_1 and P_2 are the pitches in, respectively, the bottom and the top layer; the value between the brackets is the fraction of the original pitch. D_1 is the thickness of the bottom CLC layer and D_2 is the thickness of the top CLC layer. These thicknesses were not fitted separately but calculated by using the simulated pitch and the number of pitches in the first layer. For the second layer, we used the pitch, the thickness of a single layer, and the loss of thickness in the first layer to calculate the final thickness. The refractive indices of the CLC in the first layer were changed to take a loss of density into account. We assume that the refractive index change is homogeneous over the first layer, that it is linear with the loss of density, and that the effect is the same for both n_e and n_o , as expressed in Equation (1). The parameter x was varied from 0 to 0.2 and ultimately set at 0.1 for all fits. This improved the fit and would mean that both the pitch and the refractive indices change during the deposition and curing procedure of the second layer. A change in tilt was not incorporated in our model. The number of layers per pitch was set for all simulations to 36, corresponding with a 10° rotation of the director between layers.

$$n'_e = n_e(1 - x) + x, \quad (1a)$$

$$n'_o = n_o(1 - x) + x, \quad (1b)$$

The red graph in Figure 5d is the simulation where the twist discontinuity is set to that of the red spectrum and the pitches are fitted; in the green graph the twist discontinuity is optimized as well. This allows us to verify how the model transfers from the red to the green experimental data. Fairly good fits are obtained and further discussion can be found in Section 3.3.

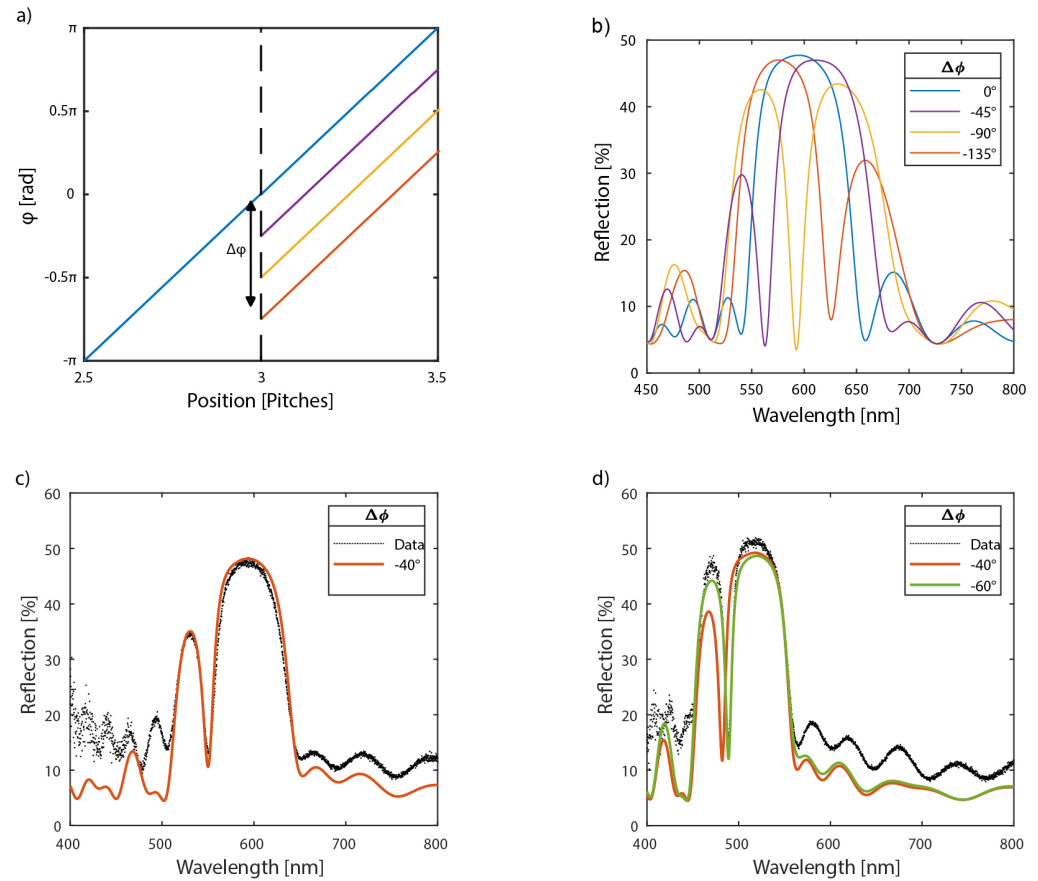


Figure 5. (a) Twist angle variation near the edge between the two layers. The colors correspond with those of the simulations in sub-figure b (b) Simulated reflection spectra for different discontinuities in the twist angle. (c) Simulated best fit reflection spectrum for the red CLC according to (b) (discontinuity -40°), together with the experimental spectrum (black). (d) Simulated best fit for the green CLC (discontinuity -60°) together with the measured spectrum.

Table 1. Best fit parameters for two CLC layers with a discontinuity in the twist angle, in order to match with the experimental data.

Parameter	Red CLC	Green CLC ¹	Green CLC
$\Delta\phi$	-40°	-40°	-60°
P1 (fraction)	382 nm (95%)	334 nm (96%)	332 nm (96%)
P2 (fraction)	360 nm (89%)	314 nm (90%)	313nm (90%)
D1 ² (#P)	1.17 μm (3.1)	1.19 μm (3.6)	1.18 μm (3.6)
D2 ² (#P)	1.41 μm (3.9)	1.39 μm (4.4)	1.40 μm (4.5)

¹ The twist discontinuity is set to the fit of the red CLC. ² Thicknesses were not fitted.

3.2.3. Defect Layer

When two CLCs with a different position of the band gap are placed on top of each other with perfect optical contact, no defect mode is observed, as explained in Section 3.2.1. But if two CLC layers with a similar band gap have a third CLC layer with shifted band gap placed between them, a defect mode will form [29]. The diffusion of the chiral dopant from

the first layer into the second layer can explain the formation of this intermediate layer. When the chiral dopant migrates to the second layer before curing, an increase in dopant concentration in the second layer is expected, leading to a decrease in pitch. The profile of the dopant concentration can be inhomogeneous and time-dependent because of diffusion. In our model, for simplicity, we assume an abrupt jump in pitch, as schematically shown in Figure 6a. To illustrate the effect of a thin intermediate layer with a different pitch, between two CLC layers with the same pitch, the spectra for three simplified cases are shown in Figure 6b. For this simulation, the refractive indices, tilt, and pitch of the CLCs are the same as before (Figure 1a) and the pitch of the intermediate layer is changed to 0.5, 0.6, and 0.7 times the pitch of the outer layer (188 nm, 226 nm, and 263 nm, respectively). The thickness of the first layer is 3 pitches, of the intermediate layer 1 pitch and of the outer layer 2 pitches. This means that the whole stack contains 6 pitches in total. The thickness of the defect layer changes between simulations because we set it as one pitch. The reflection spectrum of the stack (Figure 6b) has a notch in the band gap due to a defect mode. The pitch of the intermediate layer determines the position of the notch within the reflection band and the position shifts towards the blue with decreasing pitch.

To obtain a good fit between the experimental results and the numerical model, we use both blue shift mechanisms discussed in Section 3.2.1 for the bottom layer. The refractive indices of the bottom layer have the same shift as in the twist defect model (see Equation (1) with $x = 0.1$). We assumed that there was no tilt in any of the layers. The number of pitches of the first layer was kept equal to the best fit obtained for the single layer, respectively, 3.1 and 3.6 pitches for the red and green CLC. The thickness of the second layer was increased to account for the loss of material in the first layer (and not used as a fitting parameter). The defect layer was set to be one pitch (not accounted for in thickness of the second layer in Table 2) and the director exhibits no discontinuity in the azimuthal angle over the whole device.

To characterize and compare the change in pitch of the defect layer in our fits, we use the relative change in pitch. The relative change in pitch has the advantage of relating linearly to the relative change in chiral dopant without needing the exact value of the HTP, as the change in dopant concentration is causing the change in pitch. If the dopant remains the same, $p \times c = HTP^{-1}$ remains constant, and as a result, the relative change in pitch is the same as the relative change in concentration:

$$R_p = 2 \frac{p_1 - p_2}{p_1 + p_2} = 2 HTP^{-1} \frac{c_2 - c_1}{c_1 c_2} \times HTP \frac{c_1 c_2}{c_1 + c_2} = -2 \frac{c_1 - c_2}{c_1 + c_2} \quad (2)$$

We use the original pitch of the first layer (403 nm for the red and 347 nm for the green CLC) as p_1 .

Figure 6c,d show the fits of a defect layer for the CLCs with two spin-coated layers. Figure 6c shows the fit with the best correspondence for the red CLC, while in Figure 6d, the best corresponding fit is given in green and the spectrum with the parameters of the red CLC in red. The relevant parameters of these fits are shown in Table 2. P_{def} is the pitch of the defect mode and R_p its relative change. The other parameters are the same as in Table 1.

The simulations correspond well with the data even though we set the thickness of the defect layer arbitrarily to one pitch, made it piece-wise constant, and took those values out of the fitting procedure. This means that there will be a large number of parameter combinations that will provide a very good fit, which makes it impossible to give a quantitative explanation of the effects seen in the reflection spectra. To translate our findings to a third layer would increase the numbers of freedom even further and makes the interpretation of the fits harder. Therefore, we limit ourselves to the two-layer devices in both our models.

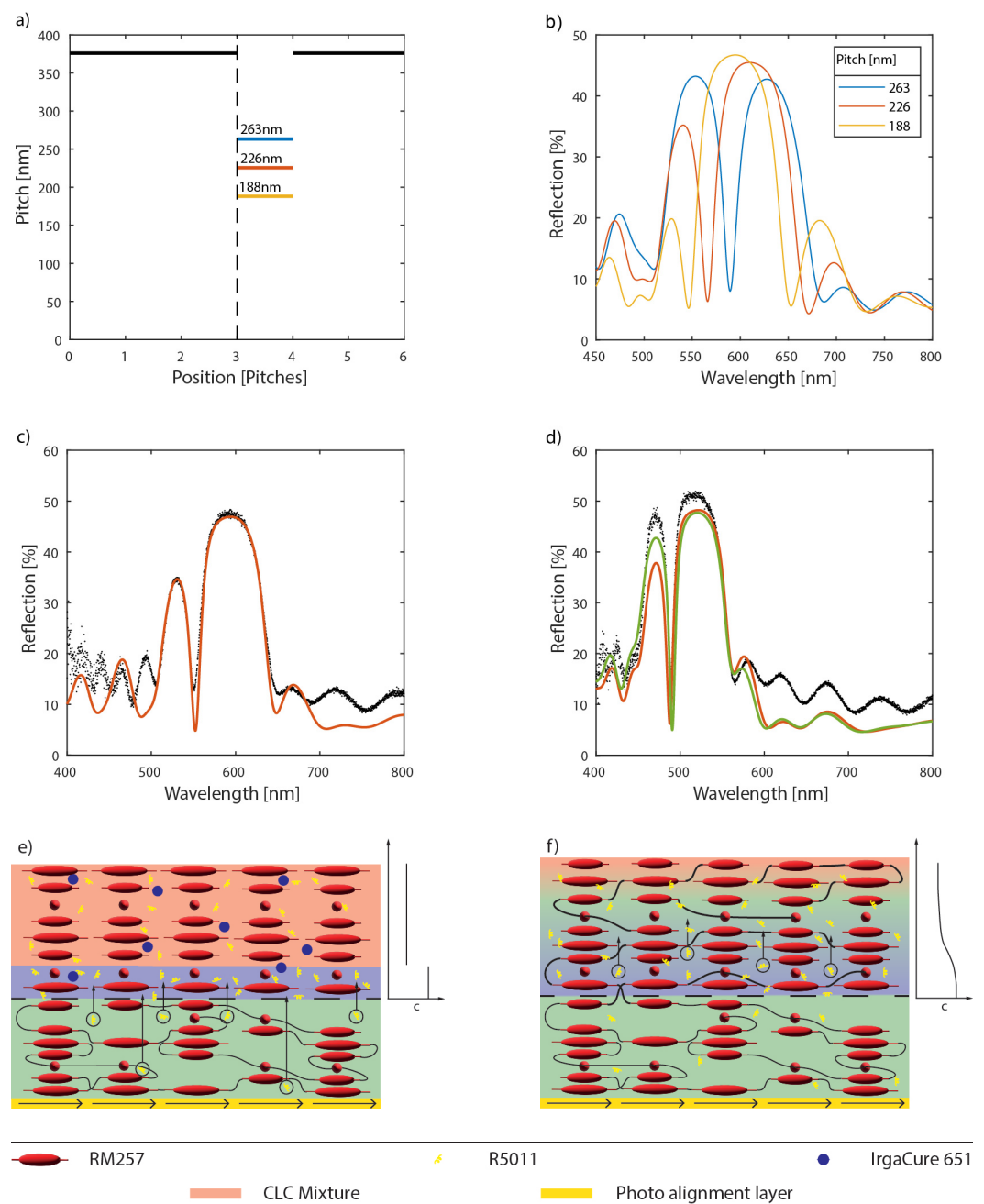


Figure 6. (a) The cross-section of the pitch profile of a CLC stack with a defect layer of different pitch. (b) Simulation of a reflection spectrum with the parameters shown in (a). (c,d) Defect modes, such as in (b), fitted to the experimental data (black). The red graphs have a relative change of dopant concentration of 0.64 and the green graph of 0.57. (e,f) Illustration of the migration of the chiral dopants in the spin-coated layer due to evaporation of the solvent (e) and diffusion (f), with a schema of the dopant concentration c as a function of the position in the layer.

Table 2. Fitted parameters of the defect layer model to match the experimental data. P: pitch, D: thickness.

Parameter	Red CLC	Green CLC ¹	Green CLC
$P_{def} (R_p)$	208 nm (0.64)	179 nm (0.64)	194 nm (0.57)
P1 (fraction)	371 nm (92%)	319 nm (92%)	319 nm (92%)
P2 (fraction)	375 nm (93%)	322 nm (93%)	322 nm (93%)
D1 ² (#P)	1.15 μm (3.1)	1.16 μm (3.6)	1.16 μm (3.6)
D2 ² (#P)	1.14 μm (3.0)	1.18 μm (3.7)	1.16 μm (3.7)

¹ The relative pitch change in the defect layer is set to the fit of the red CLC. ² Thicknesses were not fitted.

3.3. Discussion

Among the different models that have been considered in the optical simulations, we have identified two possible models that lead to a defect mode in a 2-layer sample: a discontinuity in the twist angle and an intermediate layer with different pitch. Both models can be used to obtain a reasonable fit to the experimental data.

A discontinuity in the twist angle at the interface with the second layer must originate from the surface state of the first layer after polymerization. We expect the discontinuity in the twist to be independent of the concentration of the chiral dopant. Fitting the discontinuity for the red and the green sample leads to quite different discontinuities of -40° and -60° . This difference seems substantial enough to exclude that this effect is happening.

There is a clear change in pitch in both layers and in all devices. While the pitch change in the first layer can be explained by removal of unpolymerized liquid crystal, the change in the second layer could originate from diffusion of the chiral dopant from the first layer to the second layer. If the second layer is polymerized before the chiral dopant migration from the first layer results in a uniform distribution in the second layer, a defect layer can be created due to the non-uniform chiral dopant concentration in the layers. The spectrum of the multi-layer device does not stabilize directly after the soft bake, as is evident from the difference between the samples discussed here and a quickly polymerized sample shown in the Supplementary Materials (Figure S2). This is more consistent with diffusion and the formation of a defect layer than with a twist defect because the former is a process that evolves over time whereas the latter would be set by the boundary conditions.

Because there is an important change in pitch in the defect layer and there is a minimal concentration gradient between the polymerized and the unpolymerized layer after spin-coating, we assume that the transport mechanism of the chiral dopant is initially governed by advection of the dopant as the solvent evaporates from the first layer. This causes a blue-shifted first layer and a defect layer with a much smaller pitch, while the rest of the newly spin-coated layer remains unaffected (Figure 6e). This can be seen in Figure S2, where there is a substantial broadening of the spectrum, indicating that the pitch change in the second layer remains restricted to the proximity of the interface of the two CLC layers. After this initial process, the chiral dopant diffuses further into the new layer, causing the blue shift of this layer, while diffusion back to the polymerized layer is negligible because all the solvent has been removed from it. When the second layer is polymerized in low-intensity UV light, the reactive mesogens will start cross-linking from the air interface inwards, fixing the pitch while diffusion is still ongoing. This prevents a constant pitch in the second layer, causing the defect mode to form (Figure 6f). We assume that this slow curing is also the reason that the results are repeatable because as long as the time between spin-coating and curing is not significantly increased, the extent to which the dopant can diffuse in the layer will depend on the polymerization speed. Because diffusion plays an important role in the redistribution of the dopant, a piece-wise constant doping profile is not realistic and we expect the formation of a more complex profile. Nonetheless, the model fits the experimental data well and the results are repeatable.

4. Conclusions

It is possible to spin-coat several CLC layers on top of each other with a repeatable defect mode in the band gap. Through extensive optical simulations and fitting with experimental results, we identified that the driving factor of these defects is probably inhomogeneities in the pitch due to diffusion of the chiral dopant. This diffusion can be approximated by a piece-wise constant pitch profile. This gives us more understanding of what happens between the different layers and can be used to design CLC devices while lowering the process steps.

Supplementary Materials: The following supporting information can be downloaded at: <https://www.mdpi.com/article/10.3390/cryst14030231/s1>, Figure S1: Reflection spectra of the 1-, 2-, and 3-layered blue CLC; Figure S2: Reflection spectra of a sample cured at a UV intensity of 20 mW/cm² for 5 min after 1, 2, and 3 deposited layers; Figure S3: The reflection spectra of 5 different devices: (a,b) 1 layer red and green CLC, respectively, (c,d) 2 layer red and green CLC, respectively, (e,f) 3 layers red and green CLC, respectively.

Author Contributions: Conceptualization of the experimental work, B.-H.L. and C.-T.W.; investigation, B.-H.L.; formal analysis, F.V.A. and J.B.; software, F.V.A.; supervision, C.-T.W., K.N., and J.B.; visualization, F.V.A.; writing—original draft preparation, F.V.A.; writing—review and editing, K.N. and J.B.; validation, C.-T.W., K.N. and J.B. All authors have read and agreed to the published version of the manuscript.

Funding: This research was funded by the Ministry of Science and Technology, Taiwan grant number 111-2628-E-110-001-MY2.

Data Availability Statement: The raw data supporting the conclusions of this article will be made available by the authors on request.

Conflicts of Interest: The authors declare no conflicts of interest.

References

1. Mohammadimasoudi, M.; Neyts, K.; Beeckman, J. Thin film polarizer and color filter based on photo-polymerizable nematic liquid crystal. In Proceedings of the Emerging Liquid Crystal Technologies X; Chien, L.C., Coles, H.J., Kikuchi, H., Smalyukh, I.I., Eds.; International Society for Optics and Photonics, SPIE: San Francisco, CA, USA, 2015; Volume 9384, p. 93840E.
2. Butt, M.; Khonina, S.; Kazanskiy, N. Recent advances in photonic crystal optical devices: A review. *Opt. Laser Technol.* **2021**, *142*, 107265. [[CrossRef](#)]
3. Tang, G.J.; He, X.T.; Shi, F.L.; Liu, J.W.; Chen, X.D.; Dong, J.W. Topological Photonic Crystals: Physics, Designs, and Applications. *Laser Photonics Rev.* **2022**, *16*, 2100300. [[CrossRef](#)]
4. Mitov, M. Cholesteric Liquid Crystals with a Broad Light Reflection Band. *Adv. Mater.* **2012**, *24*, 6260–6276. [[CrossRef](#)]
5. Zou, J.; Hsiang, E.L.; Zhan, T.; Yin, K.; He, Z.; Wu, S.T. High dynamic range head-up displays. *Opt. Express* **2020**, *28*, 24298–24307. [[CrossRef](#)]
6. Matsuhisa, Y.; Huang, Y.; Zhou, Y.; Wu, S.T.; Takao, Y.; Fujii, A.; Ozaki, M. Cholesteric liquid crystal laser in a dielectric mirror cavity upon band-edge excitation. *Opt. Express* **2007**, *15*, 616–622. [[CrossRef](#)]
7. Ortega, J.; Folcia, C.L.; Etxebarria, J. Upgrading the Performance of Cholesteric Liquid Crystal Lasers: Improvement Margins and Limitations. *Materials* **2018**, *11*, 5. [[CrossRef](#)]
8. Kopp, V.I.; Zhang, Z.Q.; Genack, A.Z. Lasing in chiral photonic structures. *Prog. Quantum Electron.* **2003**, *27*, 369–416. [[CrossRef](#)]
9. Mysliwiec, J.; Szukalska, A.; Szukalski, A.; Sznitko, L. Liquid crystal lasers: The last decade and the future. *Nanophotonics* **2021**, *10*, 2309–2346. [[CrossRef](#)]
10. Nys, I.; Stebryte, M.; Ussembayev, Y.Y.; Beeckman, J.; Neyts, K. Tilted Chiral Liquid Crystal Gratings for Efficient Large-Angle Diffraction. *Adv. Opt. Mater.* **2019**, *7*, 1901364. [[CrossRef](#)]
11. Ren, H.; Xu, S.; Liu, Y.; Wu, S.T. Switchable focus using a polymeric lenticular microlens array and a polarization rotator. *Opt. Express* **2013**, *21*, 7916–7925. [[CrossRef](#)]
12. Igeta, K.; Higuchi, A.; Kobashi, J.; Tomioka, Y.; Oka, S.; Yoshida, H. Tuning the Reflection Bandwidth of Polarization Volume Gratings by Guest Material Penetration. *ACS Appl. Opt. Mater.* **2023**. [[CrossRef](#)]
13. Sanz-Enguita, G.; Ortega, J.; Folcia, C.L.; Aramburu, I.; Etxebarria, J. Role of the sample thickness on the performance of cholesteric liquid crystal lasers: Experimental, numerical, and analytical results. *J. Appl. Phys.* **2016**, *119*, 073102. [[CrossRef](#)]
14. Yeh, P.; Gu, C. *Optics of Liquid Crystal Displays*, 2nd ed.; Wiley: New York, NY, USA, 2009.
15. Berreman, D.W. Optics in Stratified and Anisotropic Media: 4×4-Matrix Formulation. *J. Opt. Soc. Am.* **1972**, *62*, 502–510. [[CrossRef](#)]

16. Xue, X.; Berteloot, B.; Stebryte, M.; Neyts, K.; Beeckman, J. Role of homeotropic alignment strength at the air interface of polymerized liquid crystal layers. *Opt. Mater. Express* **2021**, *11*, 4036–4050. [[CrossRef](#)]
17. Belyakov, V.A.; Semenov, S.V. Optical defect modes in chiral liquid crystals. *J. Exp. Theor. Phys.* **2011**, *112*, 694–710. [[CrossRef](#)]
18. Ali, T.; Lin, J.D.; Snow, B.; Wang, X.; Elston, S.J.; Morris, S.M. A Thin-Film Flexible Defect-Mode Laser. *Adv. Opt. Mater.* **2020**, *8*, 1901891. [[CrossRef](#)]
19. Ozaki, M.; Ozaki, R.; Matsui, T.; Yoshino, K. Twist-Defect-Mode Lasing in Photopolymerized Cholesteric Liquid Crystal. *Jpn. J. Appl. Phys.* **2003**, *42*, L472. [[CrossRef](#)]
20. Jeong, S.M.; Ha, N.Y.; Takanishi, Y.; Ishikawa, K.; Takezoe, H.; Nishimura, S.; Suzaki, G. Defect mode lasing from a double-layered dye-doped polymeric cholesteric liquid crystal films with a thin rubbed defect layer. *Appl. Phys. Lett.* **2007**, *90*, 261108. [[CrossRef](#)]
21. Ha, N.Y.; Takanishi, Y.; Ishikawa, K.; Takezoe, H. Simultaneous RGB reflections from single-pitched cholesteric liquid crystal films with Fibonacci defects. *Opt. Express* **2007**, *15*, 1024–1029. [[CrossRef](#)]
22. Ha, N.Y.; Ohtsuka, Y.; Jeong, S.M.; Nishimura, S.; Suzaki, G.; Takanishi, Y.; Ishikawa, K.; Takezoe, H. Fabrication of a simultaneous red–green–blue reflector using single-pitched cholesteric liquid crystals. *Nat. Mater.* **2008**, *7*, 43–47. [[CrossRef](#)]
23. Ha, N.Y.; Jeong, S.M.; Nishimura, S.; Suzaki, G.; Ishikawa, K.; Takezoe, H. Simultaneous Red, Green, and Blue Lasing Emissions in a Single-Pitched Cholesteric Liquid-Crystal System. *Adv. Mater.* **2008**, *20*, 2503–2507. [[CrossRef](#)]
24. Ha, N.Y.; Jeong, S.M.; Nishimura, S.; Takezoe, H. Color-temperature tunable white reflector using bichiral liquid crystal films. *Opt. Express* **2010**, *18*, 26339–26344. [[CrossRef](#)]
25. Ha, N.Y.; Jeong, S.M.; Nishimura, S.; Takezoe, H. Color- and Reflectance-Tunable Multiple Reflectors Assembled from Three Polymer Films. *Adv. Mater.* **2010**, *22*, 1617–1621. [[CrossRef](#)] [[PubMed](#)]
26. Mohammadmasoudi, M.; Geiregat, P.; Van Acker, F.; Beeckman, J.; Hens, Z.; Aubert, T.; Neyts, K. Quantum dot lasing from a waterproof and stretchable polymer film. *Light. Sci. Appl.* **2022**, *11*, 275. [[CrossRef](#)] [[PubMed](#)]
27. Chigrinov, V.; Kwok, H.S.; Takada, H.; Takatsu, H. Photo-aligning by azo-dyes: Physics and applications. *Liq. Cryst. Today* **2005**, *14*, 1–15. [[CrossRef](#)]
28. Kopp, V.I.; Genack, A.Z. Twist Defect in Chiral Photonic Structures. *Phys. Rev. Lett.* **2002**, *89*, 033901. [[CrossRef](#)]
29. Ozaki, R.; Sanda, T.; Yoshida, H.; Matsuhisa, Y.; Ozaki, M.; Yoshino, K. Defect Mode in Cholesteric Liquid Crystal Consisting of Two Helicoidal Periodicities. *Jpn. J. Appl. Phys.* **2006**, *45*, 493. [[CrossRef](#)]

Disclaimer/Publisher’s Note: The statements, opinions and data contained in all publications are solely those of the individual author(s) and contributor(s) and not of MDPI and/or the editor(s). MDPI and/or the editor(s) disclaim responsibility for any injury to people or property resulting from any ideas, methods, instructions or products referred to in the content.